Rapid Communications | Editors' Suggestion

Large enhancement of the spin Hall effect in Mn metal by Sn doping

D. Qu,[1] T. Higo,[1,2] T. Nishikawa,[1] K. Matsumoto,[1] K. Kondou,[3] D. Nishio-Hamane,[1] R. Ishii,[1] P. K. Muduli,[1] Y. Otani,[1,2,3] and S. Nakatsuji[1,2,*]

[1]*Institute for Solid State Physics, University of Tokyo, Kashiwa 277-8581, Japan*
[2]*CREST, Japan Science and Technology Agency, Kawaguchi, Saitama 332-0012, Japan*
[3]*Center for Emergent Matter Science, RIKEN, Wako, Saitama 351-0198, Japan*

(Received 26 May 2018; revised manuscript received 19 August 2018; published 3 October 2018)

The recent discovery of the large anomalous Hall effect (AHE) in noncollinear kagome antiferromagnets Mn_3X (X = Sn, Ge) has highlighted compounds and alloys based on a combination of Mn and X. As the spin Hall effect (SHE) and AHE share the same origin, the injection of pure spin current into alloys based on Mn and X could potentially engender a large SHE. Here, we report that our spin Seebeck and the spin pumping measurements both reveal that doping Mn with 18% Sn strikingly increases the spin Hall angle of the *amorphous/nanocrystalline* Mn-Sn alloy by as much as 20 times while the resistivity is reduced by ten times compared with pure Mn. Our study not only serves as an essential reference for pure spin current phenomena in Mn-based alloys but may also offer a promising method for exploring future energy-saving spin Hall materials.

DOI: 10.1103/PhysRevMaterials.2.102001

The study of spin current and its related phenomena has attracted broad attention in the last decades. In particular, pure spin current contains only spin angular momentum but no net charge flow, and thus is expected to be beneficial for low power consumption spintronic devices [1]. The spin Hall effect (SHE) converts charge current to transverse spin current due to spin-orbit coupling [2]. Inversely, spin current can be converted to transverse charge current by the inverse spin Hall effect (ISHE), which provides an essential electrical approach to detect the pure spin current [3,4].

While extensive studies have established the SHE in heavy transition metals, magnets have been relatively less explored in terms of SHE as they are time-reversal odd. Nonetheless, several pioneering research studies have been performed for ferromagnetic metals such as Py and Co [5,6]. In addition, antiferromagnets have recently attracted much attention as the next generation active element for spintronic devices due to exceptional advantages such as high-frequency magnetization dynamics, negligible stray fields, and insensitivity to perturbation [7–12]. Among these materials, noncollinear kagome lattice antiferromagnets Mn_3X (X = Sn, Ge, Ga) have stood out prominently because of their large transverse responses to static and dynamic electric/magnetic fields. These antiferromagnets have been found to show a large anomalous Hall (AHE) [13–16], anomalous Nernst (ANE) [17,18], and a magnetic optical Kerr effect [19] despite their negligible magnetization. Moreover, the antiferromagnet Mn_3Sn has been experimentally identified as a Weyl magnet for the first time in magnets [20]. The Weyl points near the Fermi energy serve as sources and drains of the large fictitious field or Berry curvature in the momentum space, which causes the large AHE and ANE [13–18].

These discoveries have highlighted the compounds and alloys based on a combination of Mn and X in general. Since SHE/ISHE and AHE share the same origin, it is of great interest to explore spin-charge conversion in Mn-X alloys [21]. In addition, since many intriguing magnetic materials are known in Mn-based compounds, it is essential to study the ISHE in elemental Mn alone before investigating the interplay between the spin current and the magnetic configuration and the doping effects of the X elements. In this Rapid Communication, we report ISHE of both Mn and Mn-Sn amorphous/nanocrystalline thin films.

To study the ISHE in elemental Mn and Mn-Sn alloys, we employ the thermally generated pure spin current from the spin Seebeck effect (SSE) in a commercially obtained polycrystalline ferrimagnetic insulator yttrium iron garnet (YIG) substrate [22]. We also supplement this result with spin pumping (SP) measurements where pure spin current is created through coherently excited spin waves [4]. These two independent methods allow us to unambiguously determine two key parameters, namely, the spin Hall angle θ_{SH}, which evaluates the efficiency between charge and spin conversion, and the spin diffusion length λ_{sd}, which provides the measure of the average distance spin travels before losing its information. By using an insulator for spin injection, we can avoid parasitic effects from charge carriers such as anisotropic magnetoresistance, anomalous and planar Hall effects, and a shunting effect that may complicate the spin current conversion. Moreover, YIG is particularly useful as recent works have demonstrated that SSE using YIG may generate pure spin current reliably [23] and robustly regardless of its crystallinity [24].

Our analyses of the SSE measurements using a series of samples with different thicknesses have yielded a modest θ_{SH} but long λ_{sd} for Mn. In comparison, the same types of analyses and measurements for amorphous/nanocrystalline nonmagnetic $Mn_{82}Sn_{18}$ have revealed a striking enhancement

*satoru@issp.u-tokyo.ac.jp

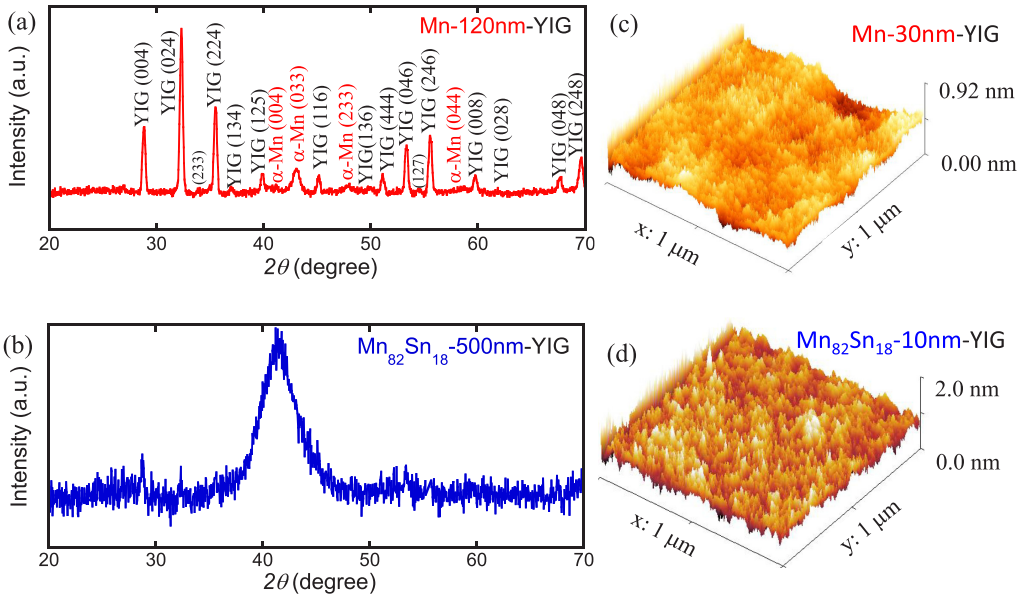

FIG. 1. Grazing angle XRD pattern for (a) Mn(120 nm)/YIG and (b) $Mn_{82}Sn_{18}$(500 nm)/YIG. Surface topography probed by AFM for (c) Mn(30 nm)/YIG and (d) $Mn_{82}Sn_{18}$(10 nm)/YIG, over an area of 1 μm × 1 μm.

of θ_{SH} by a factor of 20, while the resistivity (ρ) is reduced by about ten times. These estimations are also further confirmed by SP measurements. Our results indicate the energy consumption ($\sim\rho/\theta_{SH}^2$) of $Mn_{82}Sn_{18}$ as a spin-orbit-torque spintronic device is nearly 4000 times smaller than that for Mn [25]. Our work not only serves as an essential reference for studying the pure spin current phenomena in Mn-based alloys, but also indicates that Sn doping provides a promising method in exploring energy-efficient spin Hall materials.

The Mn and Mn-Sn alloy thin films are deposited at room temperature by magnetron sputtering onto YIG substrates from a commercially obtained Mn target or Mn_3Sn target, respectively. The details of sample fabrication are available in the Supplemental Material [26]. The YIG substrates are 0.5 mm in thickness and 10 mm × 3 mm laterally. No thermal treatment is performed. By using both inductively coupled plasma atomic emission spectroscopy (ICP-AES) and energy-dispersive spectroscopy on a scanning electron microscope (EDX-SEM), the composition of the Mn-Sn alloy is determined to be $Mn_{82}Sn_{18}$ (see Supplemental Material [26]). The stoichiometric difference between the target and thin film is often seen in oxides [27] and sometimes seen in metallic films [28].

We first examine the crystalline quality of the films using the grazing angle x-ray diffractometer (XRD) measurement. As shown in Fig. 1(a), polycrystalline YIG (marked in black) and polycrystalline α-Mn (marked in red) peaks are observed for the 120-nm-thick Mn thin film on YIG. In contrast, the $Mn_{82}Sn_{18}$ film exhibits a much broader XRD peak even for thickness of 500 nm as shown in Fig. 1(b). By using the Scherrer equation $B(2\theta) = \lambda/(A\cos\theta)$, where $B(2\theta)$ is the peak full width at half maximum, and $\lambda = 0.15418$ nm is the wavelength of the x ray using the Cu target, we estimate the grain size A to be 2 nm. This broad peak overlaps with the crystalline peaks of α-Mn, β-Sn, and several Mn-Sn alloys, therefore the $Mn_{82}Sn_{18}$ thin film deposited at room temperature could be a mixture of an amorphous and nanocrystalline structure of Mn, Sn, and Mn-Sn alloys.

We further investigated the surface morphology of the thin films on YIG by an atomic force microscope (AFM). Figures 1(c) and 1(d) show an AFM scan over a 1 μm × 1 μm area of as-deposited 30-nm Mn and 10-nm $Mn_{82}Sn_{18}$ on YIG. We found the films are notably smooth with a mean roughness of 0.07 and 0.15 nm for the Mn and $Mn_{82}Sn_{18}$ films, respectively, which is comparable to the mean roughness of 0.15 nm for the bare YIG substrate. The AFM image of the YIG substrate is shown in the Supplemental Material [26]. These results indicate high interface qualities. The resistivities of the Mn/YIG and $Mn_{82}Sn_{18}$/YIG samples were measured by the four-terminal method [Fig. 2(a)]. We find the ρ for Mn and $Mn_{82}Sn_{18}$ are about 3 and 0.3 mΩ cm, respectively. Films thinner than 30 nm showed higher resistivities caused by an increased boundary/surface scattering, as shown in the insets of Figs. 2(d) and 3(b).

Now we discuss the results for the ISHE in both Mn and $Mn_{82}Sn_{18}$ from the spin current generated by the longitudinal SSE in YIG. The schematic picture of the setup is shown in Fig. 2(b). The sample, with the film side covered with a thin and soft silicone sheet, is sandwiched between two Cu blocks. The top Cu plate is attached to a resistive heater. The bottom Cu block acts as a heat sink. Using the same geometry, the temperature gradient is simultaneously monitored during the measurement by two thermocouples placed on the top and bottom surfaces of another sample with the same dimension. Under a vertical temperature gradient and in-plane magnetic field, SSE generates a pure magnon spin current in YIG. The pure spin current is injected vertically into the attached metallic layer and is converted into charge current by ISHE. The sign of the thermal voltage determines the sign of θ_{SH} [1].

The spin-dependent thermal voltages for Mn on YIG with different Mn thicknesses are shown in Fig. 2(c). A thicker film generates smaller voltages because of finite λ_{sd} and smaller

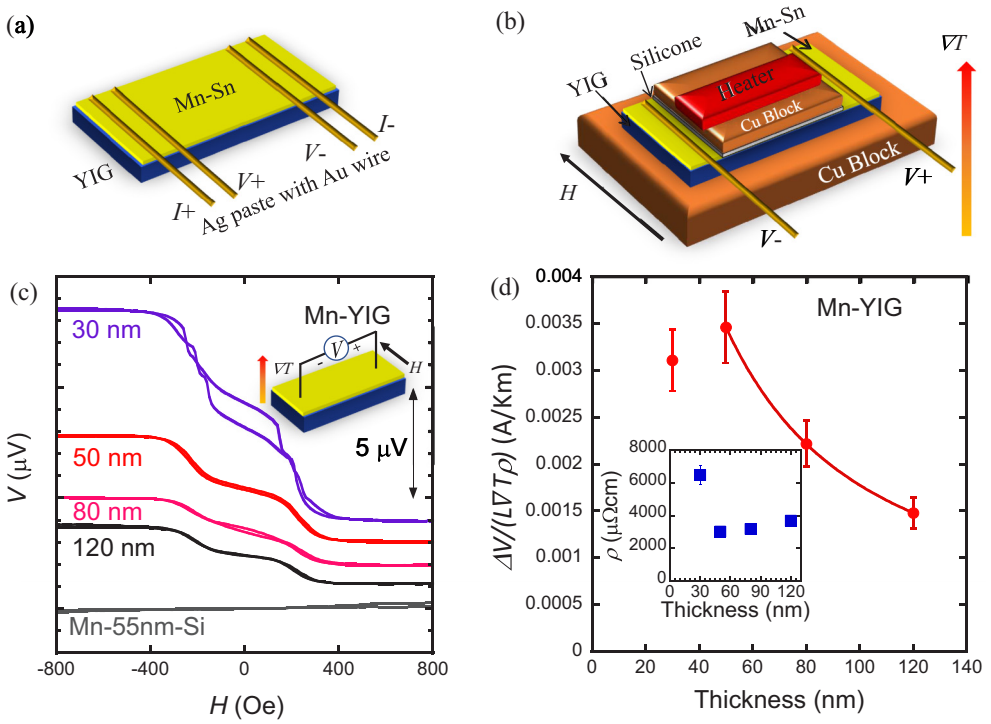

FIG. 2. Schematic illustration of (a) the four-terminal electric and (b) the thermal transport setup. (c) Magnetic field dependence of the ISHE voltage for Mn(t)/YIG and Mn(55 nm)/Si with various thicknesses t. The inset shows the schematic measurement geometry. (d) Plot of $\Delta V/(L\nabla T\rho)$ vs thicknesses for Mn(t)/YIG. The solid line is a fitting to Eq. (1). The inset is thickness-dependent resistivity.

resistance. The higher voltages in the negative saturation field indicate a negative $\theta_{\rm SH}$ for Mn opposite to the Pt case. A part of the magnetic field responses, especially the plateau observed in the low magnetic field region ($|B| < 200$ Oe), is caused by the noncollinear magnetization between surface and bulk YIG [29]. To demonstrate that the induced thermal voltage comes from the ISHE in Mn, we show that for the 55-nm-thick Mn layer on Si, no sizable ANE is observed.

The obtained ISHE voltage from the SSE spin current injection can be expressed as [30,31]

$$\Delta V(t) = 2CL\nabla T\rho(t)\theta_{\rm SH}\frac{\lambda_{\rm sd}}{t}\tanh\left(\frac{t}{2\lambda_{\rm sd}}\right). \qquad (1)$$

Here, ΔV is the voltage difference between the positive and negative saturation field, $L\approx 8$ mm is the distance between the voltage terminals, $\nabla T \approx 6\,{\rm K/mm}$ is the temperature gradient, and t is the thickness of the metal film.

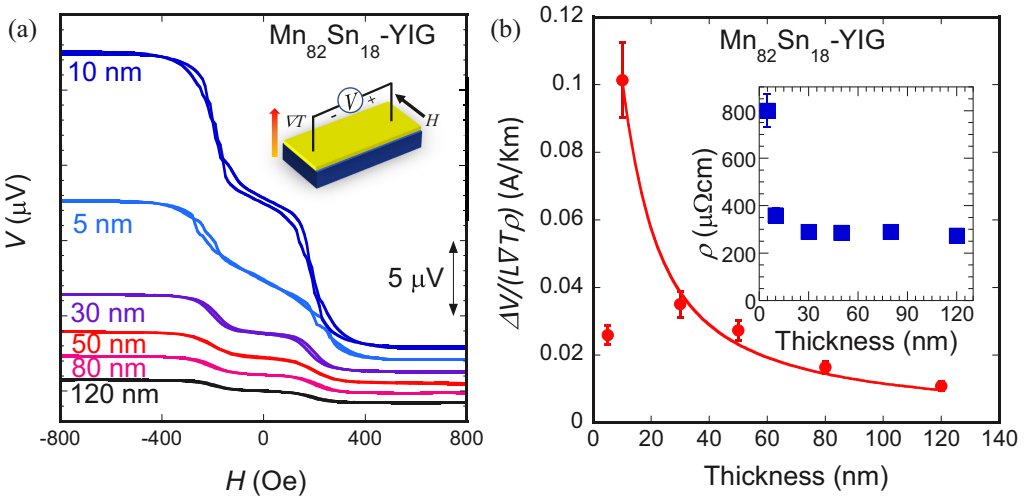

FIG. 3. (a) Thickness and magnetic field dependence of the ISHE voltage for $Mn_{82}Sn_{18}(t)$/YIG. The inset shows the schematic measurement geometry. (b) Plot of $\Delta V/(L\nabla T\rho)$ vs thicknesses for $Mn_{82}Sn_{18}(t)$/YIG. The solid line is a fitting to Eq. (1). The inset is thickness-dependent resistivity.

$C = \frac{2e}{\hbar}\frac{\gamma\hbar\rho' k_m^3 l_m}{4\pi M\pi^2}\frac{B_1 B_S}{B_2} g_{\text{eff}}^{\uparrow\downarrow} k_B$ is the spin current injection coefficient [31], containing the magnetic properties of YIG (saturation magnetization $4\pi M = 140\,\text{kA/m}$, gyromagnetic ratio $\gamma = 1.76 \times 10^{11}\,\text{s}^{-1}\,\text{T}^{-1}$, magnon diffusion length $l_m = 70\,\text{nm}$, finite ferromagnetic insulator thickness factor $\rho' \sim 1$, maximum wave number $k_m = 2 \times 10^9\,\text{m}^{-1}$, parameters from the diffusion equation $B_1 = 0.55$, $B_s = 2.2 \times 10^{-4}$, $B_2 = 5.1 \times 10^{-3}$, the Planck constant $\hbar = 1.054 \times 10^{-34}\,\text{J s}$, the electron charge $e = 1.6 \times 10^{-19}\,\text{C}$, and the Boltzmann constant $k_B = 1.38 \times 10^{-23}\,\text{J K}^{-1}$) and the spin mixing conductance ($g_{\text{eff}}^{\uparrow\downarrow}$) between the metal layer and YIG. By employing the spin mixing conductance ($g_{\text{eff}}^{\uparrow\downarrow}$) available in the literature, $g_{\text{eff}}^{\uparrow\downarrow}(\text{Mn}) = (4.5 \pm 0.4) \times 10^{18}\,\text{m}^{-2}$ [11], we estimated the spin current injection coefficient to be $C \approx 3.5\,\text{A m}^{-1}\,\text{K}^{-1}$. According to Eq. (1), we plot $\Delta V/(L\nabla T\rho)$ to estimate the θ_{SH} and λ_{sd} for Mn with different thicknesses as shown in Fig. 2(d). Excluding the first point, which drops because of possible spin current backflow, we fit our results with Eq. (1). From the fitting, we directly obtained θ_{SH} and λ_{sd} to be $\theta_{\text{SH}}(\text{Mn}) = -(0.23 \pm 0.03)\%$, $\lambda_{\text{sd}}(\text{Mn}) = 11.5 \pm 0.15\,\text{nm}$. Both θ_{SH} and λ_{sd} agree very well with the previous report for Mn [11]. The consistent results of $\theta_{\text{SH}}(\text{Mn})$ also indicate $l_m = 70\,\text{nm}$ may be a good estimation for the magnon diffusion length of our polycrystalline YIG. We noted l_m can be up to a few microns for single-crystalline YIG [32,33]. The shorter l_m in our study could be due to the higher magnon scattering rate induced by different crystal orientations in polycrystalline YIG.

Now we show that 18% Sn doping to Mn well enhances θ_{SH} by an order of magnitude. First, we find the spin-dependent thermal voltages ΔV are similar for both $Mn_{82}Sn_{18}$ and Mn, but the ρ is one order of magnitude smaller in $Mn_{82}Sn_{18}$, thus $\Delta V/(L\nabla T\rho)$ is one order of magnitude larger in $Mn_{82}Sn_{18}$. A similar magnetic field response to the Mn case confirms that the voltage also originates from the spin current generated in YIG and thus ISHE [Fig. 3(a)]. Moreover, a similar thickness dependence in $\Delta V/(L\nabla T\rho)$ is observed [Fig. 3(b)]; the 5-nm thin film has a smaller voltage due to spin current backflow. Since very similar $g_{\text{eff}}^{\uparrow\downarrow}$ has been reported for the Mn and FeMn alloys [$g_{\text{eff}}^{\uparrow\downarrow}(\text{Mn}) = (4.5 \pm 0.4) \times 10^{18}\,\text{m}^{-2}$ and $g_{\text{eff}}^{\uparrow\downarrow}(\text{FeMn}) = (4.9 \pm 0.4\,) \times 10^{18}\,\text{m}^{-2}$] with very different resistivity on the YIG substrate [11], considering the high interface quality for both Mn/YIG and $Mn_{82}Sn_{18}$/YIG films, a similar resistivity for the $Mn_{82}Sn_{18}$ and FeMn alloys (~300 $\mu\Omega\,\text{cm}$), and a robust and consistent YIG surface quality [30], we assume the same $g_{\text{eff}}^{\uparrow\downarrow}(Mn_{82}Sn_{18}) = (4.9 \pm 0.4\,) \times 10^{18}\,\text{m}^{-2}$ for comparison. By employing the same fitting shown in Fig. 3(b), we find $\theta_{\text{SH}}(Mn_{82}Sn_{18}) \approx -(4.4 \pm 0.7)\%$ and $\lambda_{\text{sd}}(Mn_{82}Sn_{18}) = 3.7 \pm 0.8\,\text{nm}$. Notably, the θ_{SH} is far more enhanced by 20 times compared with Mn. In fact, the $\theta_{\text{SH}}(Mn_{82}Sn_{18})$ could be smaller with a larger $g_{\text{eff}}^{\uparrow\downarrow}(Mn_{82}Sn_{18})$. To the best of our knowledge, the largest $g_{\text{eff}}^{\uparrow\downarrow}$ for thin metals on YIG reported is Pt/YIG with $g_{\text{eff}}^{\uparrow\downarrow}(\text{Pt}) = 6.9 \times 10^{18}\ \text{m}^{-2}$ [34], and if we assume this $g_{\text{eff}}^{\uparrow\downarrow}$ for Mn-Sn, we obtain the lower limit for $\theta_{\text{SH}}(Mn_{82}Sn_{18}) \approx -3.1\%$, which is still 14 times larger than Mn. Nevertheless, we observed an increase in the total spin to charge conversion including the interfacial transport.

To verify this striking enhancement in θ_{SH}, we further performed SP measurements on the Mn and $Mn_{82}Sn_{18}$ on polycrystalline bulk YIG samples. The samples are put onto an open coplanar waveguide (CPW) patterned on a SiO_2/Si substrate. A radio-frequency (rf) electric current of 9 GHz is passed through the CPW by a signal generator which generates an ac Oersted field applied to YIG [Fig. 4(a)]. In this configuration, an external dc magnetic field is applied parallel to CPW to cause the SP effect in the polycrystalline YIG, injecting pure spin current into the adjacent metallic layers. The films are connected to Au electrodes with Ag paste in a perpendicular direction to CPW to detect the rectified voltage generated by ISHE.

Figure 4(b) shows the ISHE voltage obtained for Pt(10)/YIG (blue), Mn(50)/YIG (orange), and $Mn_{82}Sn_{18}$(50)/YIG (green). Both Mn and $Mn_{82}Sn_{18}$ have negative voltages compared with Pt, consistent with their negative θ_{SH}. The higher resonance field and broad multiple peaks observed are most likely from the polycrystalline nature of the YIG substrate, where the latter is caused by the overlapped resonance spectra from different grains [24]. By using the symmetric Lorentzian function [4], we extract the averaged ISHE voltage from the peaks, and we confirm the expected linear increase of the ISHE voltage as a function of the rf power [Fig. 4(c)]. To obtain the θ_{SH}, we employ the following equation derived from Ref. [34],

$$\theta_{\text{SH}}(M) = \theta_{\text{SH}}(\text{Pt})\frac{V_{\text{ISHE}}(M)}{V_{\text{ISHE}}(\text{Pt})}\frac{\rho(\text{Pt})}{\rho(M)}\frac{L(\text{Pt})}{L(M)} \times \frac{\frac{\lambda_{\text{sd}}(\text{Pt})}{t(\text{Pt})}\tanh\left(\frac{t(\text{Pt})}{2\lambda_{\text{sd}}(\text{Pt})}\right)}{\frac{\lambda_{\text{sd}}(M)}{t(M)}\tanh\left(\frac{t(M)}{2\lambda_{\text{sd}}(M)}\right)}\frac{g_{\uparrow\downarrow}(\text{Pt})}{g_{\uparrow\downarrow}(M)}, \quad (2)$$

where M represents Mn or $Mn_{82}Sn_{18}$. As the bulk character of YIG (0.5 mm thick) does not allow us to determine $g_{\text{eff}}^{\uparrow\downarrow}$, we use the same $g_{\text{eff}}^{\uparrow\downarrow}(\text{Mn}) = (4.5 \pm 0.4) \times 10^{18}\,\text{m}^{-2}$ for the analysis. By further using the reported values in the literature such as $\theta_{\text{SH}}(\text{Pt}) \approx 10\%$ [34] as well as other quantities obtained in our measurement, the large enhancement of the θ_{SH} in the doped Mn is verified, namely, $\theta_{\text{SH}}(Mn_{82}Sn_{18}) \approx -(6.2 \pm 1.6)\%$, $\theta_{\text{SH}}(\text{Mn}) \approx -(0.121 \pm 0.034)\%$, which are consistent with the SSE results.

To understand the origin of the large θ_{SH} for $Mn_{82}Sn_{18}$, and to detect any contribution from nanocrystalline magnets such as ferromagnetic Mn_2Sn and noncollinear antiferromagnetic Mn_3Sn, we measured the Hall voltage for the alloy samples on YIG and Si at various temperatures down to 50 K, as shown in Figs. 5(a) and 5(b). We choose a thinner film (30 nm) on YIG and a thicker film (500 nm) on Si to probe both the interfacial and bulk contributions from $Mn_{82}Sn_{18}$/YIG and $Mn_{82}Sn_{18}$. The Hall effect is found to be mostly linear with the field and does not exhibit any hysteresis around zero field at all the temperatures measured, indicating that the large θ_{SH} is not a result of any magnetic order. A very weak nonlinear field dependence of the Hall resistivity is found for $Mn_{82}Sn_{18}$/YIG and is attributed to the spin-dependent scattering at the interface [35–37].

Given the absence of intrinsic magnetic contributions, it is reasonable to compare our observation of the enhancement in θ_{SH} with other similar doping-induced changes in θ_{SH}

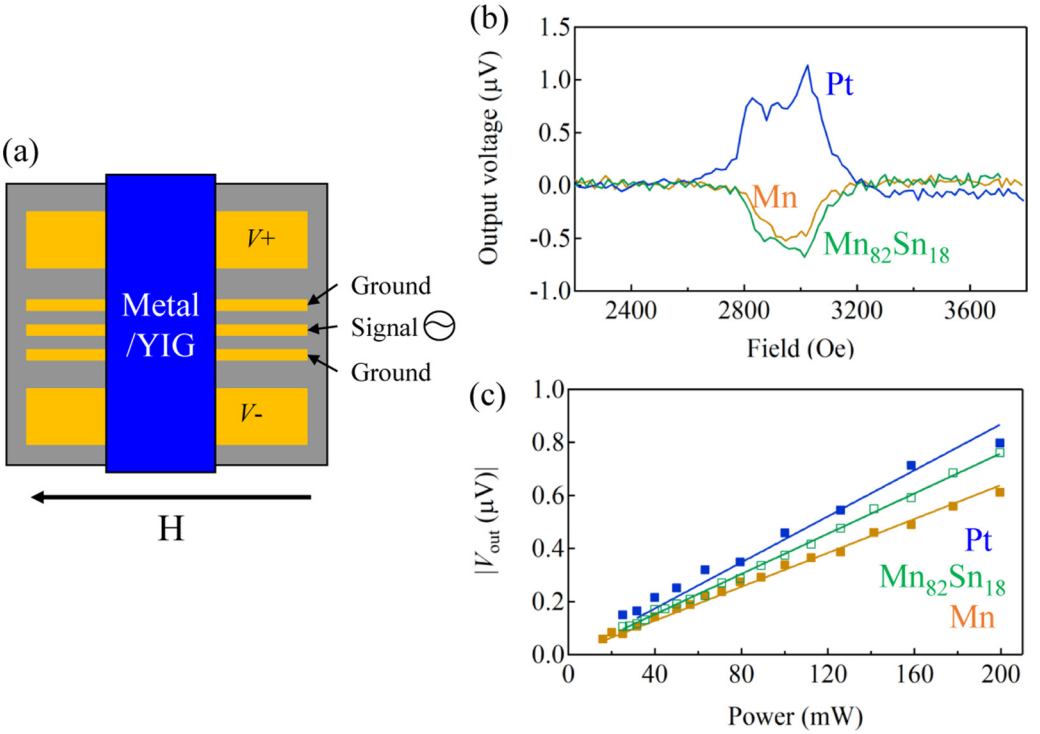

FIG. 4. (a) Schematic drawing of the CPW. (b) ISHE voltage for Pt(10)/YIG (blue), Mn(50)/YIG (orange), and $Mn_{82}Sn_{18}$/YIG (green). (c) rf power dependence of the ISHE voltage.

[38–42]. In the Cu and Au cases, the doping of heavy metals such as Bi and Ta is reported to increase θ_{SH} while reducing λ_{sd}, which has been attributed to the extrinsic mechanism, namely, the increased number of centers for skew or side-jump scattering depending on the scaling relation between ρ and spin Hall resistivity (ρ_{SH}). Thus, the observed enhancement in θ_{SH} and the reduction in λ_{sd} by the Sn doping in Mn metal may point to a similar extrinsic mechanism. In fact, θ_{SH} for Sn alone should be negligible as Sn has filled s and d shells. On the other hand, as a heavy metal, Sn may well increase the effective spin-orbit scattering rate, which is the likely origin of the enhancement in θ_{SH} as well as the reduction in λ_{sd}.

Notably, however, in the case of Sn-doped Mn, the θ_{SH} is *increased* with *reducing* ρ, distinctly different from the previous reports where θ_{SH} increases with increasing ρ [39–42]. Considering many of the high θ_{SH} materials have high ρ, our approach of doping a more conductive element in highly resistive materials may enhance the θ_{SH} while reducing their ρ. The energy consumption by spin Hall materials is proportional to ρ/θ_{SH}^2 [25], which is 4000 times larger for Mn than that for $Mn_{82}Sn_{18}$ due to a 20 times larger θ_{SH} and a ten times smaller ρ. The dramatic difference suggests this approach is beneficial for exploring energy-saving spintronic materials.

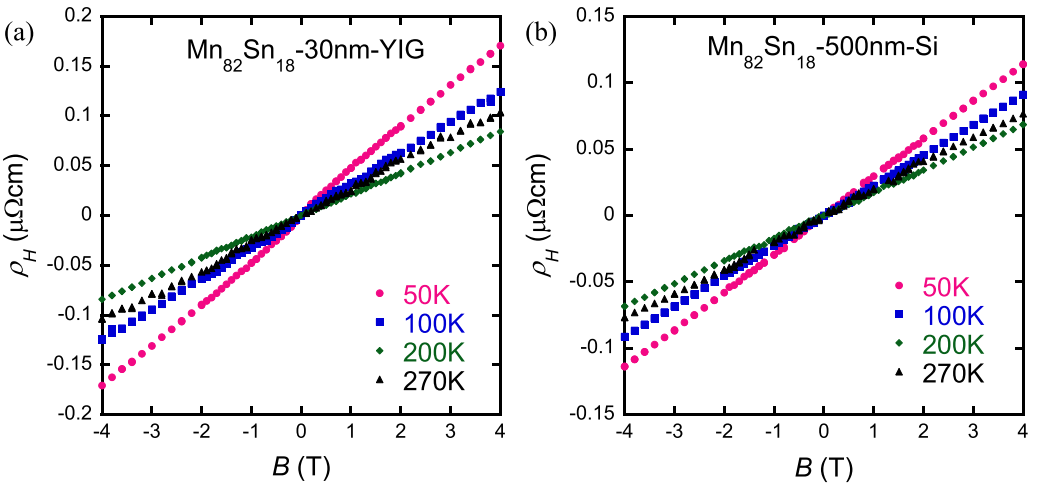

FIG. 5. Magnetic field dependence of the Hall resistivity for (a) $Mn_{82}Sn_{18}$(30 nm)/YIG and (b) $Mn_{82}Sn_{18}$(500 nm)/Si obtained at various temperatures.

It is also important to point out that although Mn has a modest θ_{SH} compared to many other transition metals, the 18% Sn-doped alloy, being amorphous/nanocrystalline and nonmagnetic, exhibits a largely enhanced θ_{SH}. This enhancement could also occur in other Mn-based alloys doped with another element. Moreover, a recent report for Au_xTa_{1-x} films has shown that θ_{SH} changes smoothly with Au concentration while the system varies from polycrystalline to amorphous/nanocrystalline structures [43]. Similarly, large θ_{SH} is also expected for Mn-Sn crystalline films. Therefore, in a study of pure spin current injection in an Mn-based alloy, one must be careful in separating the intrinsic contribution from the magnetic configuration and the extrinsic contribution by alien atoms.

To summarize, we have performed a comprehensive study on the inverse spin Hall effect in pure Mn metal and $Mn_{82}Sn_{18}$ amorphous/nanocrystalline alloys by using a combination of thermally and coherently excited spin current from YIG through the spin Seebeck and spin pumping effects. We have obtained consistent results from both measurements and estimated $\theta_{SH} \approx -0.23\%$ and -4.4%, and $\lambda_{sd} \approx 11.5$ and 3.7 nm for Mn and $Mn_{82}Sn_{18}$, respectively. The large enhancement of θ_{SH} in the Sn-doped Mn not only serves as an important reference for the study of SHE/ISHE in Mn-based alloys including the Weyl antiferromagnet Mn_3Sn, but, more importantly, it provides a viable route for enhancing θ_{SH} with reducing ρ, which is beneficial for designing energy-saving spintronic materials.

We would like to thank Dr. Yufan Li, Professor C. L. Chien, and Dr. Takumi Ohtsuki for discussions and Professor Mikk Lippmaa for the AFM support. This work is partially supported by CREST(JPMJCR15Q5), Japan Science and Technology Agency, by Grants-in-Aid for Scientific Research (16H02209), and by Grants-in-Aids for Scientific Research on Innovative Areas (15H05882, 15H05883, and 26103002) from the Ministry of Education, Culture, Sports, Science, and Technology of Japan, and Program for Advancing Strategic International Networks to Accelerate the Circulation of Talented Researchers (No. R2604) from the Japanese Society for the Promotion of Science (JSPS). D.Q. was supported by the Japan Society for the Promotion of Science (JSPS) as an international research fellow.

[1] A. Hoffmann and S. D. Bader, Phys. Rev. Appl. **4**, 047001 (2015).
[2] M. I. Dyakonov and V. I. Perel, Phys. Lett. A **35**, 459 (1971).
[3] A. Azevedo, L. H. Vilela Leão, R. L. Rodriguez-Suarez, A. B. Oliveira, and S. M. Rezende, J. Appl. Phys. **97**, 10C715 (2005).
[4] E. Saitoh, M. Ueda, H. Miyajima, and G. Tatara, Appl. Phys. Lett. **88**, 182509 (2006).
[5] B. F. Miao, S. Y. Huang, D. Qu, and C. L. Chien, Phys. Rev. Lett. **111**, 066602 (2013).
[6] D. Tian, Y. Li, D. Qu, S. Y. Huang, X. Jin, and C. L. Chien, Phys. Rev. B **94**, 020403(R) (2016).
[7] T. Jungwirth, X. Marti, P. Wadley, and J. Wunderlich, Nat. Nanotechnol. **11**, 231 (2016).
[8] W. Zhang, W. Han, S.-H. Yang, Y. Sun, Y. Zhang, B. Yan, and S. S. P. Parkin, Sci. Adv. **2**, e1600759 (2016).
[9] J. B. S. Mendes, R. O. Cunha, O. Alves Santos, P. R. T. Ribeiro, F. L. A. Machado, R. L. Rodríguez-Suárez, A. Azevedo, and S. M. Rezende, Phys. Rev. B **89**, 140406(R) (2014).
[10] W. Zhang, M. B. Jungfleisch, W. Jiang, J. E. Pearson, A. Hoffmann, F. Freimuth, and Y. Mokrousov, Phys. Rev. Lett. **113**, 196602 (2014).
[11] C. Du, H. Wang, F. Yang, and P. C. Hammel, Phys. Rev. B **90**, 140407(R) (2014).
[12] D. Qu, S. Y. Huang, and C. L. Chien, Phys. Rev. B **92**, 020418(R) (2015).
[13] S. Nakatsuji, N. Kiyohara, and T. Higo, Nature (London) **527**, 212 (2015).
[14] N. Kiyohara, T. Tomita, and S. Nakatsuji, Phys. Rev. Appl. **5**, 064009 (2016).
[15] A. K. Nayak, J. E. Fischer, Y. Sun, B. Yan, J. Karel, A. C. Komarek, C. Shekhar, N. Kumar, W. Schnelle, J. Kübler, C. Felser, and S. S. P. Parkin, Sci. Adv. **2**, e1501870 (2016).
[16] G.-Y. Guo and T.-C. Wang, Phys. Rev. B **96**, 224415 (2017).
[17] M. Ikhlas, T. Tomita, T. Koretsune, M.-T. Suzuki, D. Nishio-Hamane, R. Arita, Y. Otani, and S. Nakatsuji, Nat. Phys. **13**, 1085 (2017).
[18] X. Li, L. Xu, L. Ding, J. Wang, M. Shen, X. Lu, Z. Zhu, and K. Behnia, Phys. Rev. Lett. **119**, 056601 (2017).
[19] T. Higo, H. Man, D. B. Gopman, L. Wu, T. Koretsune, O. M. J. van't Erve, Y. P. Kabanov, D. Rees, Y. Li, M.-T. Suzuki, S. Patankar, M. Ikhlas, C. L. Chien, R. Arita, R. D. Shull, J. Orenstein, and S. Nakatsuji, Nat. Photonics **12**, 73 (2018).
[20] K. Kuroda, T. Tomita, M.-T. Suzuki, C. Bareille, A. A. Nugroho, P. Goswami, M. Ochi, M. Ikhlas, M. Nakayama, S. Akebi, R. Noguchi, R. Ishii, N. Inami, K. Ono, H. Kumigashira, A. Varykhalov, T. Muro, T. Koretsune, R. Arita, S. Shin, T. Kondo, and S. Nakatsuji, Nat. Mater. **16**, 1090 (2017).
[21] Y. Zhang, Y. Sun, H. Yang, J. Železný, S. P. P. Parkin, C. Felser, and B. Yan, Phys. Rev. B **95**, 075128 (2017).
[22] K. Uchida, H. Adachi, T. Ota, H. Nakayama, S. Maekawa, and E. Saitoh, Appl. Phys. Lett. **97**, 172505 (2010).
[23] D. Qu, S. Y. Huang, J. Hu, R. Wu, and C. L. Chien, Phys. Rev. Lett. **110**, 067206 (2013).
[24] F.-J. Chang, J. G. Lin, and S.-Y. Huang, Phys. Rev. Mater. **1**, 031401(R) (2017).
[25] J. Han, A. Richardella, S. A. Siddiqui, J. Finley, N. Samarth, and L. Liu, Phys. Rev. Lett. **119**, 077702 (2017).
[26] See Supplemental Material at http://link.aps.org/supplemental/10.1103/PhysRevMaterials.2.102001 for details of the sample fabrication and characterization.
[27] T. I. Selinder, G. Larsson, U. Helmersson, P. Olsson, J.-E. Sundgren, and S. Rudner, Appl. Phys. Lett. **52**, 1907 (1988).
[28] S. Wurmehl, J. T. Kohlhepp, H. J. M. Swagten, B. Koopmans, C. G. F. Blum, V. Ksenofontov, H. Schneider, G. Jakob, D. Ebke, and G. Reiss, J. Phys. D: Appl. Phys. **42**, 084017 (2009).
[29] P.-H. Wu and S.-Y. Huang, Phys. Rev. B **94**, 024405 (2016).

[30] D. Qu, S. Y. Huang, B. F. Miao, S. X. Huang, and C. L. Chien, Phys. Rev. B **89**, 140407(R) (2014).

[31] S. M. Rezende, R. L. Rodríguez-Suárez, R. O. Cunha, A. R. Rodrigues, F. L. A. Machado, G. A. Fonseca Guerra, J. C. Lopez Ortiz, and A. Azevedo, Phys. Rev. B **89**, 014416 (2014).

[32] A. Kehlberger, U. Ritzmann, D. Hinzke, E.-J. Guo, J. Cramer, G. Jakob, M. C. Onbasli, D. H. Kim, C. A. Ross, M. B. Jungfleisch, B. Hillebrands, U. Nowak, and M. Kläui, Phys. Rev. Lett. **115**, 096602 (2015).

[33] L. J. Cornelissen, J. Liu, R. A. Duine, J. Ben Youssef, and B. J. van Wees, Nat. Phys. **11**, 1022 (2015).

[34] H. L. Wang, C. H. Du, Y. Pu, R. Adur, P. C. Hammel, and F. Y. Yang, Phys. Rev. Lett. **112**, 197201 (2014).

[35] S. Y. Huang, X. Fan, D. Qu, Y. P. Chen, W. G. Wang, J. Wu, T. Y. Chen, J. Q. Xiao, and C. L. Chien, Phys. Rev. Lett. **109**, 107204 (2012).

[36] C. Tang, P. Sellappan, Y. Liu, Y. Xu, J. E. Garay, and J. Shi, Phys. Rev. B **94**, 140403(R) (2016).

[37] S. S.-L. Zhang and G. Vignale, Phys. Rev. Lett. **116**, 136601 (2016).

[38] M. Gradhand, D. V. Fedorov, P. Zahn, and I. Mertig, Phys. Rev. B **81**, 245109 (2010).

[39] Y. Niimi, M. Morota, D. H. Wei, C. Deranlot, M. Basletic, A. Hamzic, A. Fert, and Y. Otani, Phys. Rev. Lett. **106**, 126601 (2011).

[40] A. Fert and P. M. Levy, Phys. Rev. Lett. **106**, 157208 (2011).

[41] Y. Niimi, Y. Kawanishi, D. H. Wei, C. Deranlot, H. X. Yang, M. Chshiev, T. Valet, A. Fert, and Y. Otani, Phys. Rev. Lett. **109**, 156602 (2012).

[42] P. Laczkowski, Y. Fu, H. Yang, J.-C. Rojas-Sánchez, P. Noel, V. T. Pham, G. Zahnd, C. Deranlot, S. Collin, C. Bouard, P. Warin, V. Maurel, M. Chshiev, A. Marty, J.-P. Attané, A. Fert, H. Jaffrès, L. Vila, and J.-M. George, Phys. Rev. B **96**, 140405(R) (2017).

[43] D. Qu, S. Y. Huang, G. Y. Guo, and C. L. Chien, Phys. Rev. B **97**, 024402 (2018).